

Single crystals of superconducting SmFeAsOH_x : Structure and properties

A. Pisoni,^{1,*} S. Katrych,¹ A. Arakcheeva,¹ T. Verebéli,² M. Bokor,² P. Huang,¹ R. Gaál,¹ P. Matus,¹ J. Karpinski,¹ and L. Forró¹

¹*Institute of Physics, EPFL, CH-1015 Lausanne, Switzerland*

²*Institute for Solid State Physics and Optics, Wigner Research Centre for Physics of the Hungarian Academy of Science, P.O. Box 49, H-1525 Budapest, Hungary*

(Received 21 March 2016; published 29 July 2016)

We report the synthesis, structure, and superconducting properties of single crystals of SmFeAsOH_x . The crystals were grown at high pressure and high temperature using a cubic anvil technique. ¹H-NMR studies confirm the presence of H atoms in the samples. Single crystal x-ray diffraction analyses demonstrate a remarkable disorder in the Sm_2O_2 layers induced by hydrogen incorporation and reveal that the H positions are compatible with a H_2O -like geometry inside the crystals. We have measured the magnetotransport properties of SmFeAsOH_x single crystals with $x = 0.07, 0.11$, and 0.16 in magnetic field up to 16 T, oriented along the two main crystallographic directions. The results show an increase of the critical temperature with hydrogen content. The zero-temperature upper critical fields and the magnetic anisotropy are calculated as a function of the hydrogen content. SmFeAsOH_x crystals present significantly higher upper critical fields and magnetic anisotropies compared to $\text{SmFeAsO}_{1-x}\text{F}_x$ compounds.

DOI: [10.1103/PhysRevB.94.024525](https://doi.org/10.1103/PhysRevB.94.024525)

I. INTRODUCTION

High-temperature superconductivity in iron-based compounds keeps puzzling the scientific community. Since the discovery of superconductivity in $\text{LaFeAsO}_{1-x}\text{F}_x$ [1] in 2008, a lot of effort has been devoted to achieve superconducting temperatures (T_c) above the nitrogen boiling point. However, the record $T_c = 58.1$ K in $\text{SmFeAsO}_{1-x}\text{F}_x$ seems to set the upper limit in this class of materials [2]. Superconductivity in LnFeAsO ($\text{Ln} = \text{lanthanide}$) compounds (also known as 1111) can be induced by external pressure or chemical doping when the magnetic and the structural transitions in the parent compound are suppressed. Carrier doping can be obtained by atomic substitution in the FeAs conducting layer or in the LnO spacing layer. In the latter case, fluorine has been mainly used to replace oxygen in the form of an F^- anion, providing an extra electron to the structure. The disadvantage of using fluorine as a doping agent is related to its low solubility in $\text{LnFeAsO}_{1-x}\text{F}_x$ materials ($x < 0.2$) that limits the study of their phase diagram in the overdoped region. Hydrogen can overcome this limit by expanding the solubility level up to $x = 0.53$ [3,4]. Many resemblances have been observed between F and H doping in LaFeAsO at low doping levels [5]. Hanna *et al.* [4] studied the effect of H doping in SmFeAsO polycrystalline samples, revealing that hydrogen optimizes the crystal structure and acts as an effective electron dopant. In particular, they reported an increase of T_c in $\text{SmFeAsO}_{1-x}\text{H}_x$ for $0 < x \leq 0.2$ with an optimal value of $T_c = 55$ K around $x = 0.2$. For $0.2 < x < 0.4$ the critical temperature decreases with hydrogen content, indicating an electron overdoping regime that cannot normally be achieved by fluorine doping.

Several possible scenarios have been suggested concerning the form in which hydrogen is incorporated into the structure of 1111 compounds. According to Miyazawa *et al.* [6], hydrogen is intercalated as an H^+ ion and attracts O^{2-} or

As^{3-} ions, causing a comprehensive decrease of the lattice parameters. However, neutron powder diffraction and first principles calculations have shown that hydride ions (H^-) tend to replace oxygen according to $\text{O}^{2-} \rightarrow \text{H}^- + e^-$ and they stably locate close to the Fe atoms, attracting negatively charged FeAs layers [4,7]. This causes a shrinkage of all the lattice constants and induces more regular FeAs₄ tetrahedrons favoring an increase of T_c [7]. On the other hand, Muraba *et al.* [8] have recently suggested that hydrogen coming from H_2O and H_2 molecules could be introduced into the oxygen vacancy site.

Here, we report the growth and the characterization of single crystals of H-incorporated SmFeAsO . We show that, according to our NMR results and the single crystal XRD analysis, the right formula of our compounds is SmFeAsOH_x rather than $\text{SmFeAsO}_{1-x}\text{H}_x$. We measured the electrical resistivity (ρ) and the upper critical field (H_{c2}) of SmFeAsOH_x single crystals with $x = 0.07, 0.11$, and 0.16 in magnetic field up to 16 T oriented parallel and perpendicular to the crystallographic c axis. The superconducting magnetic anisotropy, $\gamma_H = H_{c2}^{ab}/H_{c2}^c$, and the coherence lengths (ξ) are calculated as functions of H content.

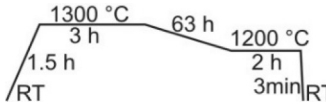
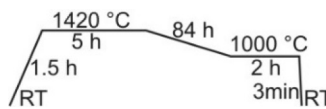
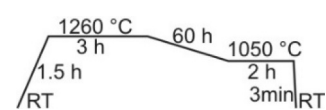
II. EXPERIMENTAL DETAILS

Single crystals of SmFeAsOH_x , with dimensions between 50 and 80 μm , were grown at 3 GPa in a cubic multianvil system from a mixture of Fe, As, SmAs, FeO, and $\text{Sm}(\text{OH})_3 \times \text{H}_2\text{O}$ (Sigma Aldrich) (in molar ratio 9:1:15.67:7.67:1, respectively) thoroughly grounded with a flux in a agate mortar inside a glovebox. Different time/temperature profiles and fluxes were used for the crystal growth, as schematically shown in Table I.

A single crystal structure study was performed on the basis of the x-ray diffraction (XRD) data collected with a Bruker diffractometer (Mo $K\alpha$ radiation, $\lambda = 0.71073 \text{ \AA}$) equipped with a CCD detector. The data reduction was performed with the APEX2 software package [9] and the structure was

*Corresponding author: andrea.pisoni@epfl.ch

TABLE I. Summary of the different time/temperature profiles and different fluxes used for the growth of SmFeAsOH_x single crystals with different hydrogen contents.

| Flux | Flux/sample ratio (weight) | Time/temperature profile ^a | Estimated final composition |
|------|----------------------------|--|-----------------------------|
| NaCl | 0.93 |  | $\text{SmFeAsOH}_{0.07}$ |
| KI | 1.17 |  | $\text{SmFeAsOH}_{0.11}$ |
| KCl | 0.7 |  | $\text{SmFeAsOH}_{0.16}$ |

^aTime in hours (h) or minutes (min); RT: room temperature.

refined and analyzed using the JANA2006 [10] software. The position of hydrogen and the structural distortion caused by its incorporation were revealed from the residual electron density calculated after the main structure model refinements on the basis of a Fourier analysis by applying $(F_{\text{experimental}} - F_{\text{calculated}})$ structural amplitude for each hkl reflection.

The lattice constants of SmFeAsOH_x were determined by powder x-ray diffraction of each synthesis product. The results were compared with those already available in the literature for $\text{SmFeAsO}_{1-x}\text{H}_x$ compounds [4]. Powder x-ray diffraction profiles were measured with a Rigaku Miniflex powder diffractometer (Cu $K\alpha$ radiation $\lambda = 1.5425 \text{ \AA}$).

In order to confirm the presence of hydrogen inside the samples, we performed wide-line ^1H -NMR measurements employing a Bruker AVANCE III NMR spectrometer at a frequency of 82.4 MHz. The inhomogeneity of the magnetic field was less than 2 ppm. The samples were placed in Teflon capsules. Free induction decay (FID) signals were collected using a 90° pulse length of $2.5 \mu\text{s}$. The collected signals were dead-time compensated and Fourier transformed. To eliminate the background contribution, an empty capsule was also measured and its spectrum was subtracted from the spectra of the investigated samples.

The electrical resistivity (ρ) was measured in a standard four-point configuration as a function of temperature from 300 K down to 1.7 K in different magnetic fields up to 16 T. Conducting leads were deposited on the surface of the samples using ion-assisted platinum deposition by focused ion beam (FIB) technology. The magnetic field was applied both parallel and perpendicular to the Fe_2As_2 layers. In our analysis of the upper critical field, we define the midpoint T_c as the temperature at which the resistivity drops 50% of its value just above the transition. The zero-point T_c is defined at the zero-resistivity point [i.e., when the measured $\rho(T)$ drops below our experimental sensitivity].

III. RESULTS AND DISCUSSION

A. Hydrogen content

Several single crystals of SmFeAsOH_x were accurately selected from each batch and the corresponding ^1H -NMR spectra were recorded (Fig. 1). Each spectrum has a Gaussian-

like peak characterized by a full width at half maximum (FWHM) of around 1-1.5 mT (500-800 ppm) and confirms the presence of hydrogen in all the investigated samples. The observed peaks are one order of magnitude narrower than those reported by Miyazawa *et al.* for $\text{LaFeAsO}_{1-x}\text{H}_x$ compounds [6]. This implicates that in our case there is no wide distribution of transferred hyperfine field from the Fe atoms, hence the H atoms are not located in proximity to the Fe atoms. However, the linewidths that we obtained in SmFeAsOH_x compounds are slightly broader than what we expect from the H atoms situated in a regular crystallographic site (range of 100 ppm), suggesting some local disorder caused by the H incorporation. Integration of the NMR spectra in Fig. 1 gives H-content values that are in quite good agreement with those reported in the legend. However, due to the very small dimensions of the samples grown, we cannot exclude that secondary phases containing hydrogen were measured by NMR, together with the selected samples. This prevents an exact determination of x from our NMR data.

We estimated the hydrogen content of our samples from the measurement of the a and c lattice parameters. Figure 2 shows

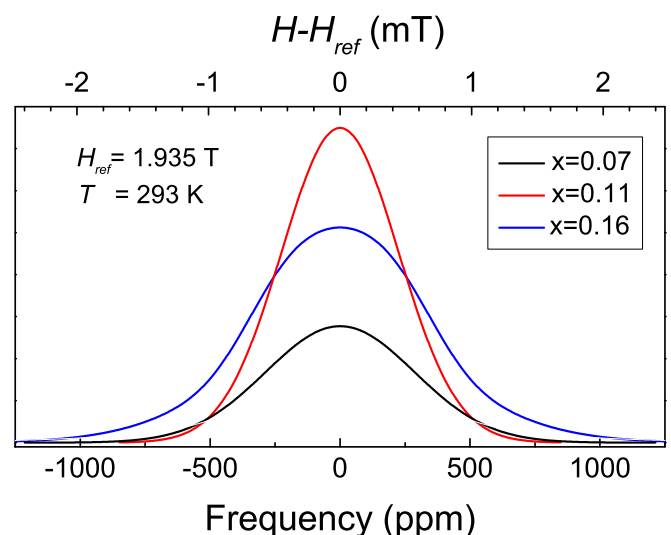


FIG. 1. Wide-line ^1H -NMR spectra of SmFeAsOH_x ($x = 0.07, 0.11, 0.16$) samples at ambient temperature in $H_{\text{ref}} = 1.935 \text{ T}$.

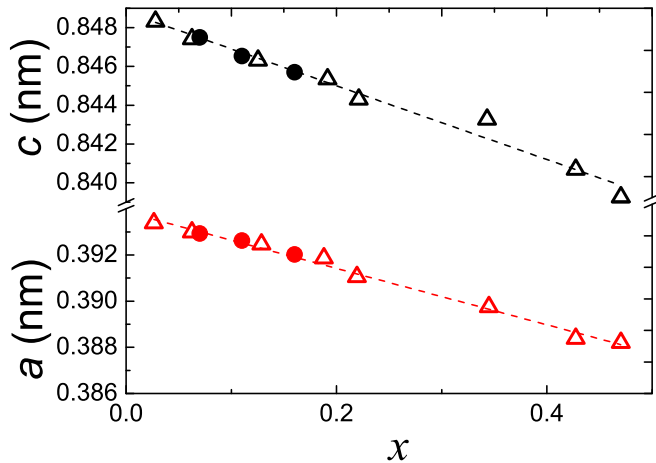


FIG. 2. Dependence of the c (black symbols) and a (red symbols) lattice parameters on the hydrogen content (x). The solid dots correspond to the results obtained by x-ray powder diffraction for the samples investigated in this work. The open triangles are the results for polycrystalline H-doped SmFeAsO reported by Hanna *et al.* [4]. The dashed lines are linear fits to the results extracted from the literature [4].

the a and c lattice parameter dependences on the hydrogen content (x) for polycrystalline SmFeAsO $_{1-x}$ H $_x$ as reported by Hanna *et al.* [4] (open triangles). The dashed lines are linear fits to the data [4]. The measured a and c lattice parameters of SmFeAsOH $_x$ are included in the same plot (solid dots). Assuming that the lattice constants of the two compounds are the same, we can extract the corresponding x value for SmFeAsOH $_x$ samples. As it will be shown below, the estimated values of x for SmFeAsOH $_x$ agree with the behavior of T_c vs x observed for SmFeAsO $_{1-x}$ H $_x$ [Fig. 6(d)] and the structural analysis confirms $x = 0.16$ as the highest doping level we obtained. The estimated final compositions of our SmFeAsOH $_x$ single crystals are reported in Table I.

B. Structure analysis

The grown SmFeAsOH $_{0.16}$ sample revealed a high crystallographic quality with a mosaic spread of $\sim 1^\circ$ (Fig. 3). Residual electron density maps, obtained by the single crystal x-ray diffraction data structure refinements, were used to compare the structure of SmFeAsOH $_{0.16}$ with that of SmFeAsO. Both structures were refined within the harmonic approximation of the atomic displacements and are presented in Fig. 4. In both compounds, the residual electron density, calculated after subtraction of the Sm, Fe, As, and O contributions, shows some significant maxima located along the fourfold axis close to Sm. For the undoped crystal [Fig. 4(a)] these maxima have been successfully fitted by an anharmonic approximation of atomic displacements, which essentially improved the reliability index R from 4.02% to 2.69%. In order to exclude the possibility that the residual electron density near the Sm atoms could arise from truncation effects, we adopted difference Fourier maps employing a weighting scheme of Fourier map calculations as described in Ref. [11]. The standard uncertainties of the experimental and calculated Fourier maps were identical for every reflection and the whole

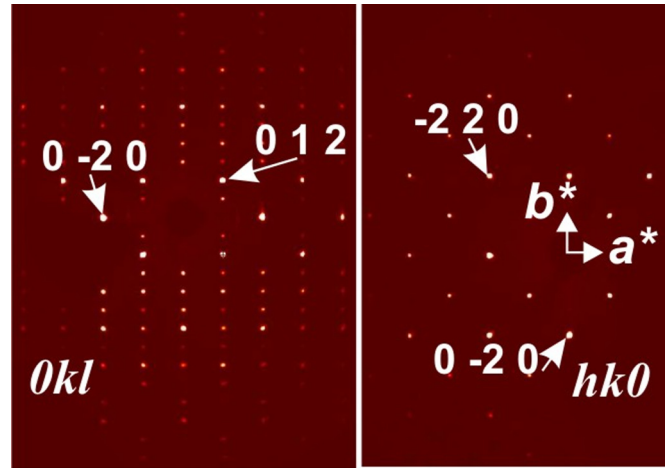


FIG. 3. The reconstructed $(0kl)$ and $(hk0)$ reciprocal space sections for SmFeAsOH $_{0.16}$ single crystal. Well-resolved reflections confirm the high quality of the single crystal used for the structural study.

sphere of reciprocal space was taken into account during the calculation. Similar to many other works dedicated to the H-atom localization from x-ray experiments, we assume by H a center of the electron cloud. Correspondingly, the O-H distance of 1.09(5) Å is a distance between the center of the O-related electron cloud and the center of a maximum in the residual electron density. This value is similar to all the O-H distances reported for H $_2$ O on the basis of the x-ray experiments.

The structure of SmFeAsO is shown in Fig. 5(a), together with the atomic displacements. SmFeAsOH $_{0.16}$ also shows some maxima near the O positions and more distant maxima near Sm [Fig. 4(b)]. Only a partial splitting of the Sm and O positions in addition to an anharmonic approximation of their atomic displacement can fit those maxima. A combination of the partial atomic splitting and the anharmonic atomic displacements improves the reliability index R from 2.18% to 1.96% in this case. It is important to note that the sum of the main and the split O position occupancies, 0.92(2) and 0.08(2), respectively, is equal to 1, i.e., the O deficiency seems to be a quasideficiency indeed. The structure of SmFeAsOH $_{0.16}$ is shown in Fig. 5(b), with the atomic displacements indicated by ellipsoids. The residual electron density map also contains some maxima [indicated as H1, H2, and H3 in Fig. 4(b)], which can be assumed to be associated with H atoms, as they are located at 1.09(5) Å from the O positions with a H-O-H angle equal to $104 \pm 1^\circ$, a typical value for the H $_2$ O molecule. The main and split positions of O, Sm, and H are only partially and alternatively occupied, so that the statistical distribution of H $_2$ O molecules can be represented with acceptable interatomic distances. One of the many possible local atomic distributions is shown in Fig. 5(c) as an example. The occupation of the proposed H positions can be estimated from the obtained structural data in the following way. If each split O atom with refined occupation 0.08(2) is connected by two H atoms, then 0.16(4) H atoms are present near the O. The number of H atoms connected by the main O position is limited by the number of split Sm atoms, which is equal to 0.02(1). Hence,

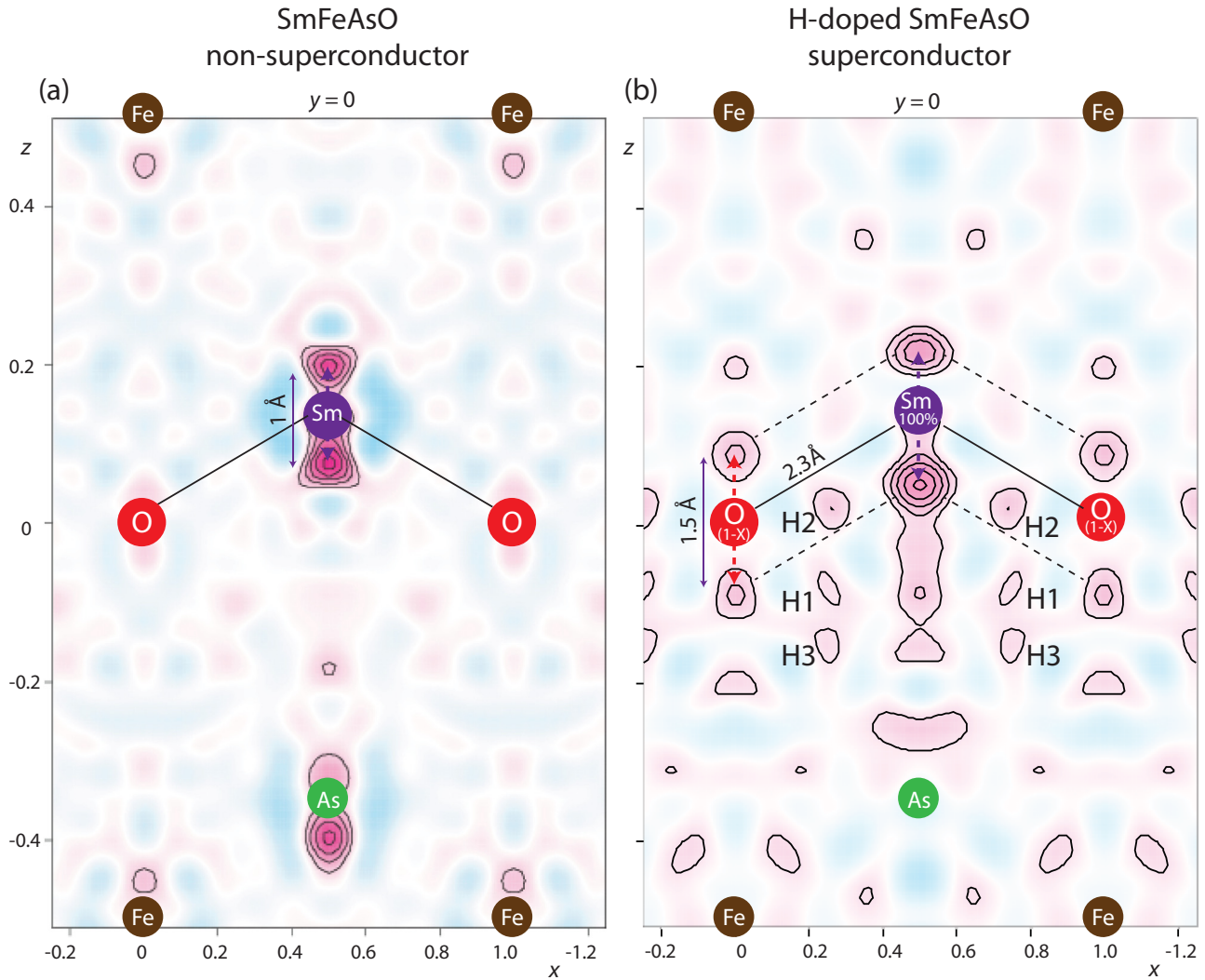


FIG. 4. Comparative analysis of the undoped and H-incorporated SmFeAsO using residual electron density mapping. The $x0z$ sections containing all essential maxima are shown for the (a) undoped and (b) H-doped crystal structures. The sections have been calculated within the harmonic approximation after subtracting the contributions from Sm, Fe, As, and O atoms. Light blue and light red background regions indicate the negative and positive areas. The highest maxima are underlined by isocurves, which are drawn with steps of 2 and $0.5 e \text{ \AA}^{-3}$ in (a) and (b), respectively. In (b), the H1, H2, and H3 maxima are very probably associated with the position of the H atoms.

about 0.04(2) H can be expected near the main O position. Therefore, the estimation leads to $x = 0.20(6)$ H atoms per SmFeAsO unit formula, and it well agrees with the value of $x = 0.16$ obtained from the dependence of the lattice constants on hydrogen content [4] (Fig. 2) [12,13].

C. Electrical resistivity

The temperature-dependent electrical resistivity of SmFeAsOH $_x$ crystals for $x = 0.07$, 0.11 , and 0.16 is shown in Figs. 6(a)–6(c), respectively. The lower-right-hand inset in each panel is a detailed view around the superconducting transition region. The upper-left-hand inset represents a scanning electron microscope (SEM) image of each sample contacted by FIB: The samples are highlighted in violet and the conducting leads in green. The value of $\rho(300 \text{ K}) \sim 0.8 \text{ m}\Omega \text{ cm}$, observed for all three samples, does not appear to show any dependence on the different hydrogen contents. However, the residual

resistance ratio (RRR) shows a nonmonotonous behavior with x , first increasing from 2.8 at $x = 0.07$ to 4 at $x = 0.11$, and then decreasing to 3.2 at $x = 0.16$. The residual resistivity values of the SmFeAsOH $_x$ single crystals studied seem to be larger than those reported by Muraba *et al.* [8] for polycrystalline SmFeAsO $_{1-x}$ H $_x$ compounds. However, we explain such an apparently incoherent result as a consequence of errors in the exact measurement of the geometrical factor, necessary to convert resistance into resistivity, due to the very small dimensions of the samples. The temperature dependence of ρ in the normal state shows an increasing nonlinear behavior with hydrogen content, approaching a $\sim T^{0.3}$ dependence at $x = 0.16$. Figure 6(d) displays the midpoint T_c of the single crystals studied in this work (red point) as a function of H content in comparison to the results obtained by Hanna *et al.* [4] for the polycrystalline samples (black triangle). The results appear in very good agreement with each other. The critical temperature of the single crystals increases from 33

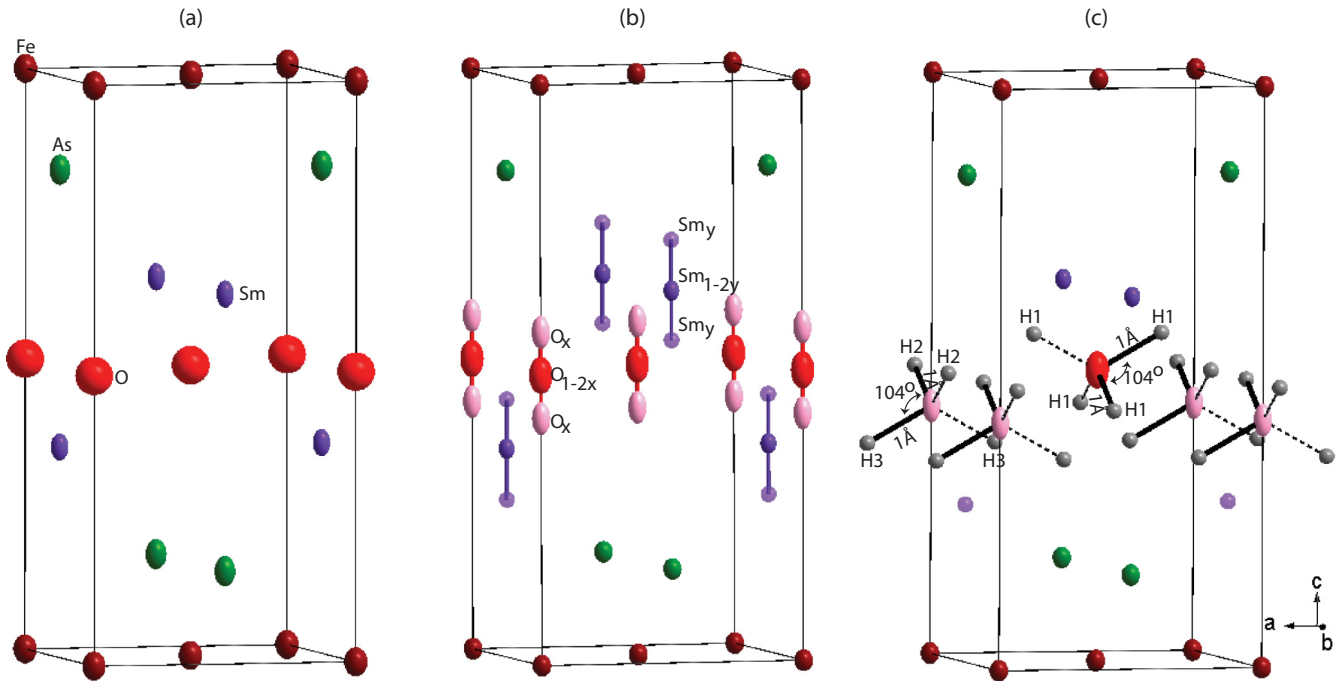


FIG. 5. Atomic distribution in a unit cell of (a) undoped and (b), (c) H-doped SmFeAsO samples. Atoms are represented with 100% probability ellipsoids. The red and the violet ellipsoids indicate the calculated positions of the O and Sm atoms, with an occupation of 0.92 and 0.98, respectively. The pink and the light violet ellipsoids represent alternative atomic positions. The estimated positions of the H atoms, H1, H2, and H3, are shown in (c), which illustrates a possible local distribution of the atoms compatible with the interatomic distances. Solid and dashed lines represent two alternative H₂O molecules for each O position.

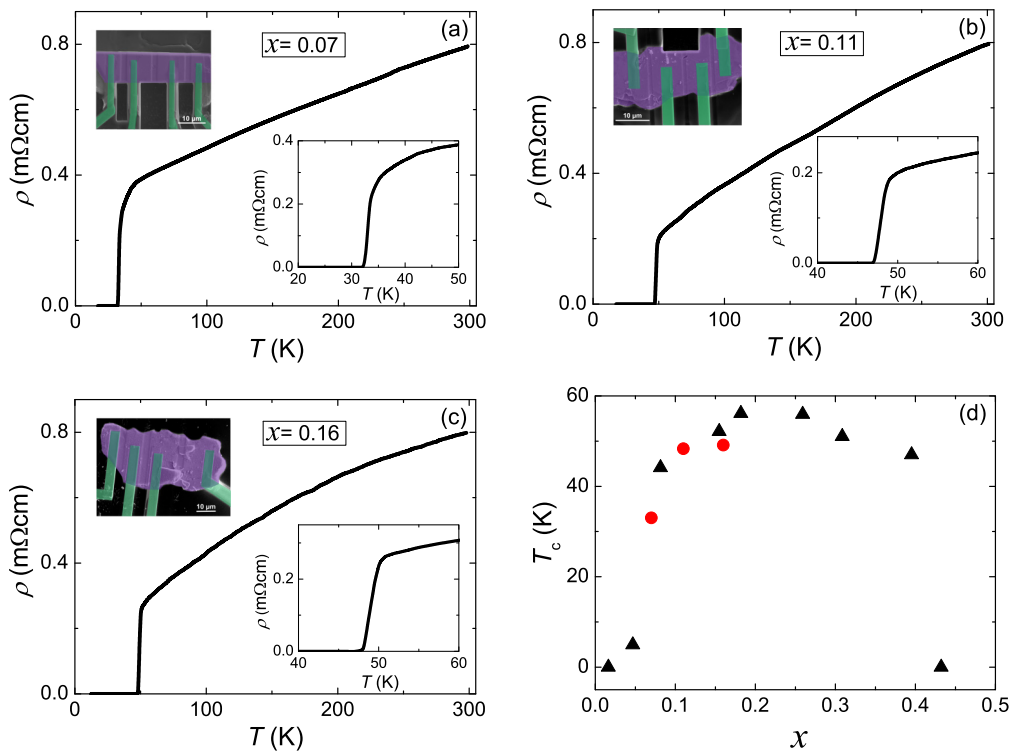


FIG. 6. Temperature dependence of resistivity of SmFeAsOH_x single crystals for (a) $x = 0.07$, (b) $x = 0.11$, and (c) $x = 0.16$. The lower-right-hand inset in each panel is a detailed view around the superconducting transition. The upper-left-hand inset presents a SEM image of the samples contacted by FIB: The samples are highlighted in violet and the platinum leads in green. (d) displays the midpoint critical temperature of the single crystals studied in this work (red points) compared to the results for polycrystalline samples reported in Ref. [4] (black triangles) as a function of hydrogen doping.

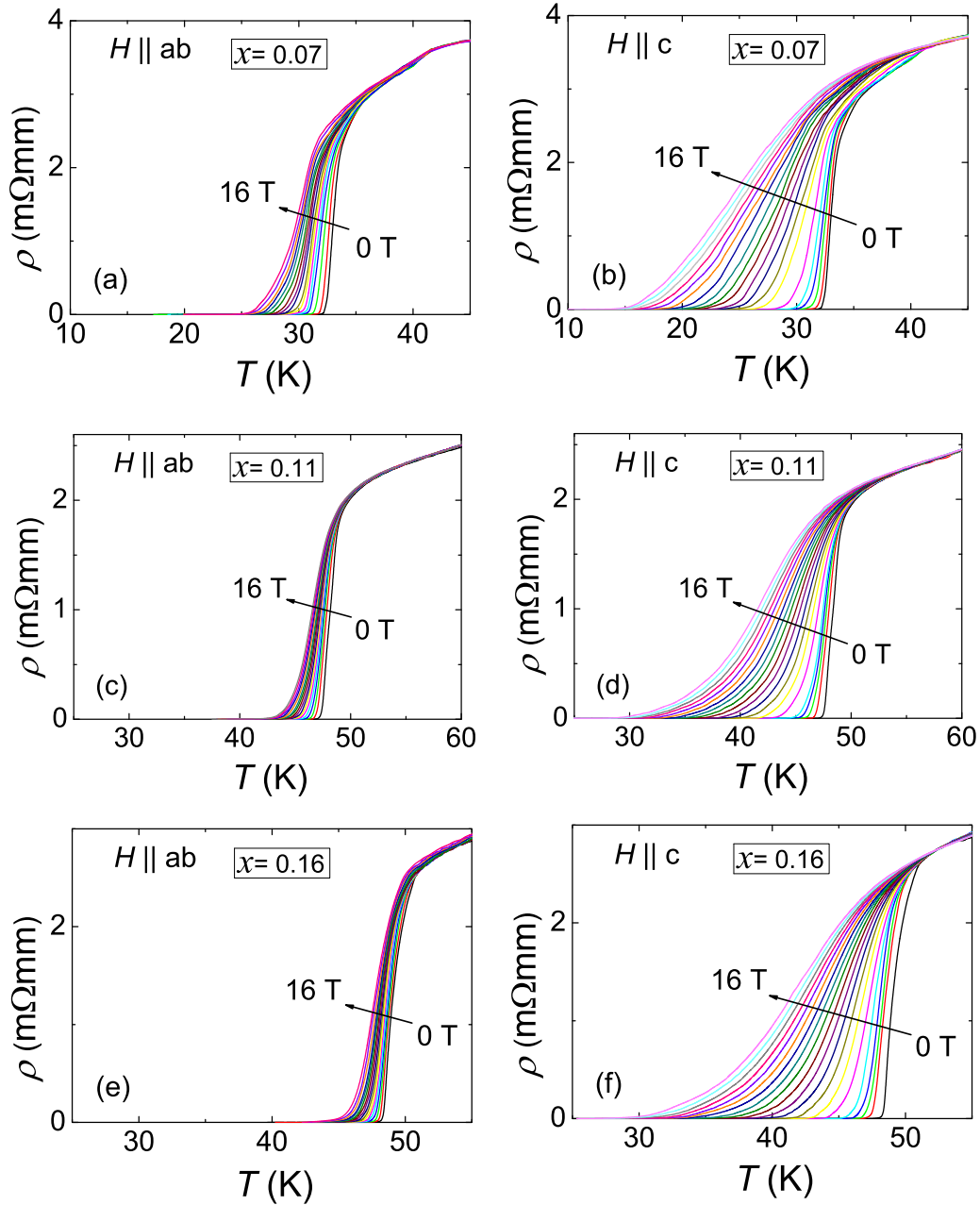


FIG. 7. Temperature and magnetic field dependence of the resistivity of SmFeAsOH_x single crystals measured with fields applied parallel to the FeAs layers ($H \parallel ab$) and perpendicular to them ($H \parallel c$). The values of the magnetic field are 0, 0.25, 0.5, 1, 2, 3, 4, 5, 6, 7, 8, 9, 10, 11, 12, 13, 14, 15, and 16 T following the arrow in the panels. Each row of panels represents the results obtained for the doping level reported on the left-hand side of the figures.

to 48.3 and 49.1 K, passing from $x = 0.07$ to 0.11 and 0.16, respectively.

D. Upper critical field

The upper critical field (H_{c2}) of the different SmFeAsOH_x crystals was evaluated by $\rho(T)$ measurements at different constant magnetic fields up to 16 T. The results for magnetic field oriented perpendicular to the crystallographic c axis ($H \parallel ab$) and parallel to it ($H \parallel c$) at different doping levels are reported in Fig. 7. With increasing magnetic field, T_c monotonously decreases, showing the expected

suppression of superconductivity. In analogy to other layered high-temperature superconductors, the shift of T_c to lower temperatures is more pronounced when $H \parallel c$ than when $H \parallel ab$, and the width of the superconducting transition monotonically increases with the magnetic field [14–18].

Figures 8(a)–8(c) present the temperature dependence of H_{c2} for $H \parallel ab$ (blue dots) and $H \parallel c$ (red dots) with $x = 0.07$, 0.11, and 0.16, respectively. The upper critical field is defined at the midpoint T_c and it is presented with solid dots. The open dots correspond to the values of H_{zero} defined at the zero-resistivity point. The temperature dependence of the in-plane (H_{c2}^{ab}) and out-of-plane (H_{c2}^c) upper critical field

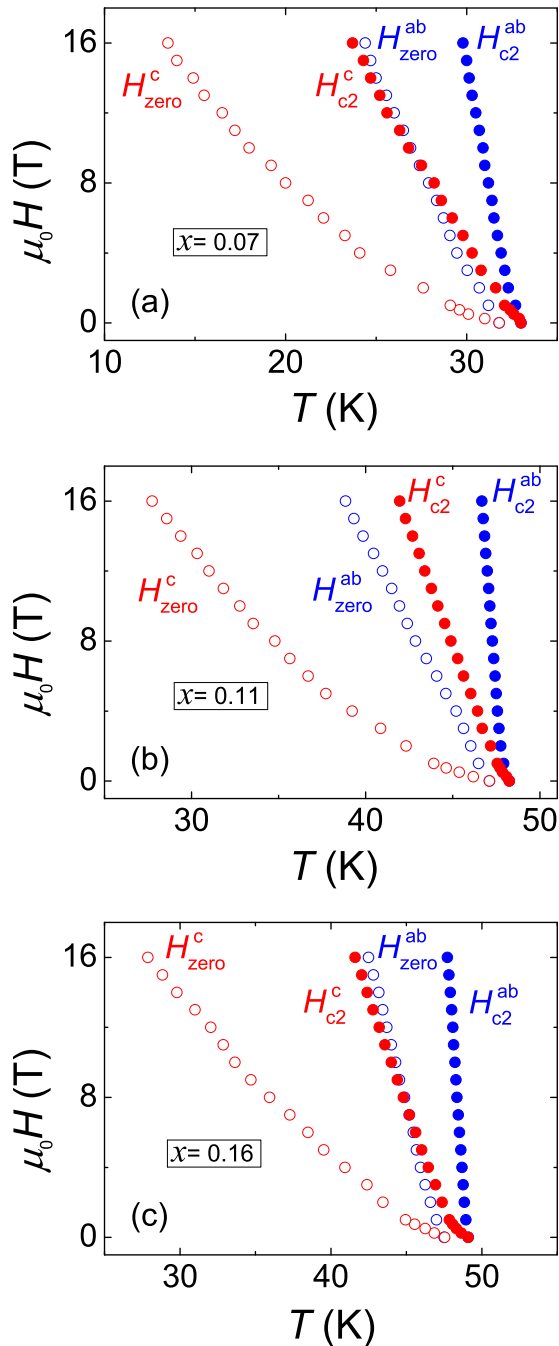


FIG. 8. Upper critical magnetic field as a function of temperature extracted from resistivity measurements with $H||ab$ (blue points) and $H||c$ (red points) for (a) $x = 0.07$, (b) $x = 0.11$, and (c) $x = 0.16$. Solid dots correspond to values of H_{c2} estimated from the midpoint of the resistive transitions while open dots represent the fields evaluated at the zero-resistivity point.

shows the same behavior already observed in other 1111 superconducting compounds [14]: a nonlinear trend with a concave curvature that is more pronounced for $H||c$ than for $H||ab$. This dependence was interpreted as an intrinsic feature of pnictide superconductors due to their multiband superconducting nature [17].

An analysis of the upper critical field can provide information about the dominant pair-breaking mechanism. In type-II

TABLE II. Superconducting parameters of SmFeAsOH_x single crystals obtained from the analysis of temperature-dependent upper critical fields shown in Fig. 8.

| x | T_c^{mid} (K) | $\mu_0 H_{c2}^{ab}$ (T) | $\mu_0 H_{c2}^c$ (T) | $\mu_0 H_{c2}^P$ (T) | ξ_{ab} (Å) | ξ_c (Å) | γ_H |
|------|---------------------------|----------------------------|-------------------------|-------------------------|-------------------|----------------|------------|
| 0.07 | 33 | 120 | 39 | 61 | 29 | 9.4 | 2.4 |
| 0.11 | 48.3 | 379 | 66 | 89 | 22.3 | 4 | 4 |
| 0.16 | 49.1 | 418 | 77 | 90 | 20.6 | 3.8 | 12 |

superconductors, pair breaking can be achieved, by application of a magnetic field, through an orbital or paramagnetic effect. The orbital effect is due to the Lorentz force that acts on the charges and the opposite momenta of the paired electrons while the paramagnetic (or spin) effect is due to Zeeman splitting of the spin singlet Cooper pairs. An approximate estimation of the zero-temperature orbital limiting field is provided by the Werthamer-Helfand-Hohenberg (WHH) theory [19] as $H_{c2}(0) = -0.69T_c(dH_{c2}/dT)_{T_c}$. In order to decide which pair-breaking effect is dominating in SmFeAsO_{1-x}H_x, we compare the value of $H_{c2}^o(0)$ to the Pauli limiting field (H_{c2}^P), defined as the critical field at which the Zeeman energy equals the superconducting condensation energy [15,20]. The Pauli or Clogston-Chandrasekhar theory [21,22] gives an approximate estimation of $H_{c2}^P(0) = 1.84T_c$. From $H_{c2}^o(0)$ we extract the in-plane and out-of-plane coherence lengths according to $\mu_0 H_{c2}^{ab}(0) = \Phi_0/(2\pi\xi_{ab}\xi_c)$ and $\mu_0 H_{c2}^c(0) = \Phi_0/(2\pi\xi_{ab}^2)$, where ξ_{ab} is the in-plane coherence length, ξ_c the out-of-plane coherence length, and Φ_0 the magnetic flux quantum. The magnetic field anisotropy was calculated near T_c from the measured midpoint H_{c2} (solid dots in Fig. 8) as $\gamma_H = H_{c2}^{ab}/H_{c2}^c$, as a function of hydrogen content. The results for each doping level and for different magnetic field orientations are summarized in Table II.

As it can be seen, the value of H_{c2}^P for every sample is much higher than $H_{c2}^o(0)$ for fields oriented along the c -axis direction while it is much smaller than $H_{c2}^o(0)$ for fields parallel to the ab planes. This indicates that the upper

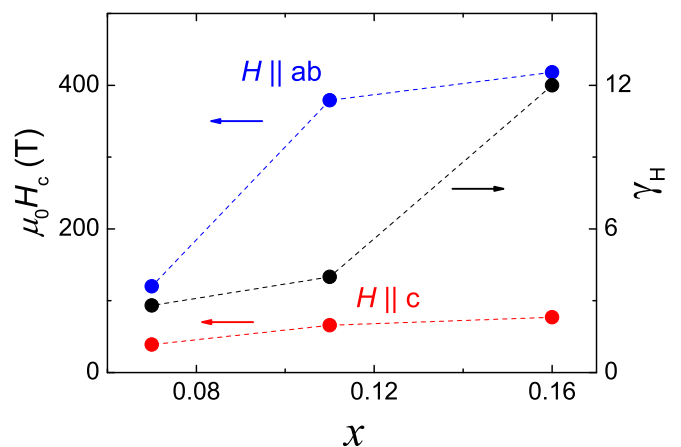


FIG. 9. In-plane (blue dots) and out-of-plane (red dots) zero-temperature upper critical field as a function of hydrogen doping. The values are extracted using the WHH formalism as described in the text. The black points correspond to the values of the magnetic field anisotropy (right axis). The dashed lines are guides to the eyes.

critical field appears to be limited by an orbital effect along the c axis and by a paramagnetic effect in the perpendicular direction. This observation is in perfect agreement with what has been reported for $\text{SmFeAsO}_{0.8}\text{F}_{0.2}$ single crystals [23]. Hydrogen doping in SmFeAsO , therefore, does not affect the physics of the limiting magnetic field compared to the F-doped compound. However, SmFeAsOH_x samples show significantly higher values of zero-temperature upper critical fields (e.g., up to four times higher along the ab direction [22]) and of magnetic anisotropy [14] than the fluorine-doped counterpart. Figure 9 shows the evaluated $H_{c2}^c(0)$ (red points) and $H_{c2}^{ab}(0)$ (blue points) as a function of hydrogen content. The magnetic field anisotropy is also presented in the same figure (right axis) in black points as a function of x . The zero-temperature upper critical field increases with hydrogen doping along both directions and starts to saturate as x approaches the optimum value of 0.2, while γ_H appears to increase more than linearly with x , in contrast to the results for polycrystalline $\text{SmFeAsO}_{1-x}\text{F}_x$, where γ_H tends to saturate to 3.5 for $0.15 < x < 0.2$ [14].

IV. CONCLUSIONS

In conclusion, we have reported the growth, structure, and superconducting properties of single crystals of SmFeAsOH_x . Three different compositions, namely, $x = 0.07$, 0.11 , and 0.16 , were obtained. The presence of H inside the crystals was confirmed by wide-line $^1\text{H-NMR}$ measurements, which also revealed some structural disorder caused by hydrogen incorporation. The a and c lattice parameters decrease with

increasing hydrogen content, in very good agreement with the results reported for polycrystalline H-doped samples. The midpoint critical temperature increases with x passing from $T_c = 33$ K at $x = 0.07$ to $T_c = 49.1$ K at $x = 0.16$. To further investigate the effect of hydrogen incorporation, we performed a detailed comparative analysis between the undoped SmFeAsO and the $\text{SmFeAsOH}_{0.16}$ crystal structures. The results display a remarkable disorder in the Sm_2O_2 layer caused by H inclusion and reveal the very probable H positions which are found to be associated with the formation of H_2O molecules within the SmFeAsOH_x crystals. Resistivity measurements in magnetic fields up to 16 T, oriented parallel and perpendicular to the FeAs planes, show values of the zero-temperature upper critical field that are significantly higher than those reported in fluorine-doped samples of the same compound. From the magnetotransport analysis we were able to extract some superconducting parameters such as the coherence lengths and the magnetic field anisotropy. The magnetic anisotropy of SmFeAsOH_x is much higher than that of $\text{SmFeAsO}_{1-x}\text{F}_x$ and it does not appear to saturate for $0.15 < x < 0.2$, as observed in the F-doped compounds.

ACKNOWLEDGMENTS

Discussions with B. Náfrádi, G. Kriza, and V. Petricek are highly acknowledged. This work was supported by the Swiss National Science Foundation (Projects No. 140760, No. 156012, No. 138053, No. 160765, and No. 166298).

A.P. and S.K. contributed equally to this work.

-
- [1] Y. Kamihara, T. Watanabe, M. Hirano, and H. Hosono, *J. Am. Chem. Soc.* **130**, 3296 (2008).
- [2] M. Fujioka, S. J. Denholme, T. Ozaki, H. Okazaki, K. Deguchi, S. Demura, H. Hara, T. Watanabe, H. Takeya, and T. Yamaguchi, *Supercond. Sci. Technol.* **26**, 085023 (2013).
- [3] S. Iimura, S. Matsuishi, H. Sato, T. Hanna, Y. Muraba, S. W. Kim, J. E. Kim, M. Takata, and H. Hosono, *Nat. Commun.* **3**, 943 (2012).
- [4] T. Hanna, Y. Muraba, S. Matsuishi, N. Igawa, K. Kodama, S.-i. Shamoto, and H. Hosono, *Phys. Rev. B* **84**, 024521 (2011).
- [5] G. Lamura, T. Shiroka, P. Bonfà, S. Sanna, R. De Renzi, F. Caglieris, M. Cimberle, S. Iimura, H. Hosono, and M. Putti, *J. Phys.: Condens. Matter* **26**, 295701 (2014).
- [6] K. Miyazawa, S. Ishida, K. Kihou, P. Shirage, M. Nakajima, C. Lee, H. Kito, Y. Tomioka, T. Ito, and H. Eisaki, *Appl. Phys. Lett.* **96**, 072514 (2010).
- [7] H. Nakamura and M. Machida, *Physica C: Superconductivity* **471**, 662 (2011).
- [8] Y. Muraba, S. Iimura, S. Matsuishi, and H. Hosono, *Inorg. Chem.* **54**, 11567 (2015).
- [9] Computer code APEX2 version 2009.9 (Bruker AXS, Madison, WI, 2009).
- [10] V. Petricek, M. Dusek, and L. Palatinus, *Z. Kristallogr.* **229**, 345 (2014).
- [11] C. Davis, E. Maslen, and J. Varghese, *Acta Crystallogr., Sect. A: Cryst. Phys., Diffr., Theor. Gen. Crystallogr.* **34**, 371 (1978).
- [12] Further details of the crystal structure investigations may be obtained from Fachinformationszentrum Karlsruhe, 76344 Eggenstein-Leopoldshafen, Germany; FAX: 49 7247-808-666; crysdata@fiz-karlsruhe.de, <http://www.fiz-karlsruhe.de/> on quoting the ICSD numbers 43006 and 431005 for H-doped $\text{SmFeAsOH}_{0.16}$ and undoped SmFeAsO , respectively (alternatively, see the Supplemental Material [13]).
- [13] See Supplemental Material at <http://link.aps.org/supplemental/10.1103/PhysRevB.94.024525> for the structural details in the crystallographic information files (CIFs) about H-doped $\text{SmFeAsOH}_{0.16}$ and undoped SmFeAsO .
- [14] J. Karpinski, N. Zhigadlo, S. Katrych, Z. Bukowski, P. Moll, S. Weyeneth, H. Keller, R. Puzniak, M. Tortello, and D. Daghero, *Physica C: Superconductivity* **469**, 370 (2009).
- [15] Y. Jo, J. Jaroszynski, A. Yamamoto, A. Gurevich, S. Riggs, G. Boebinger, D. Larbalestier, H. Wen, N. Zhigadlo, and S. Katrych, *Physica C: Superconductivity* **469**, 566 (2009).
- [16] J. Jaroszynski, S. C. Riggs, F. Hunte, A. Gurevich, D. C. Larbalestier, G. S. Boebinger, F. F. Balakirev, A. Migliori, Z. A. Ren, W. Lu, J. Yang, X. L. Shen, X. L. Dong, Z. X. Zhao, R. Jin,

- A. S. Sefat, M. A. McGuire, B. C. Sales, D. K. Christen, and D. Mandrus, *Phys. Rev. B* **78**, 064511 (2008).
- [17] J. Jaroszynski, F. Hunte, L. Balicas, Y.-J. Jo, I. Raičević, A. Gurevich, D. C. Larbalestier, F. F. Balakirev, L. Fang, P. Cheng, Y. Jia, and H. H. Wen, *Phys. Rev. B* **78**, 174523 (2008).
- [18] A. Pisoni, S. Katrych, P. Szirmai, B. Náfrádi, R. Gaál, J. Karpinski, and L. Forró, *J. Phys.: Condens. Matter* **28**, 115701 (2016).
- [19] N. Werthamer, E. Helfand, and P. Hohenberg, *Phys. Rev.* **147**, 295 (1966).
- [20] A. Gurevich, *Rep. Prog. Phys.* **74**, 124501 (2011).
- [21] A. M. Clogston, *Phys. Rev. Lett.* **9**, 266 (1962).
- [22] B. S. Chandrasekhar, *Appl. Phys. Lett.* **1**, 7 (1962).
- [23] H.-S. Lee, M. Bartkowiak, J.-H. Park, J.-Y. Lee, J.-Y. Kim, N.-H. Sung, B. K. Cho, C.-U. Jung, J. S. Kim, and H.-J. Lee, *Phys. Rev. B* **80**, 144512 (2009).